Research paper

The suitability of a low temperature post-IR IRSL signal for dating alluvial and colluvial "cut and fill" sequences in the Great Karoo, South Africa

C.J. Oldknow [a,*], A.S. Carr [b], J.M. Hooke [a], Z. Shen [c]

[a] Department of Geography and Planning, Roxby Building, University of Liverpool, L69 7ZT, UK
[b] School of Geography, Geology, and the Environment, Bennett Building, University of Leicester, LE1 7RH, UK
[c] Department of Marine Science, Coastal Carolina University, USA

ARTICLE INFO

ABSTRACT

Alluvial and colluvial "cut and fill" deposits preserved in valleys of the Karoo, South Africa, reflect basin-scale adjustments in fluvial process-regime. Such deposits in the Wilgerbosch catchment have previously proven difficult to date using radiocarbon (^{14}C) and optically stimulated luminescence (OSL) methods. In this paper, we test the suitability of K-feldspar post-IR infrared (pIRIR) methods on 19 samples from Africanders Kloof, a low-order tributary of the Sundays River. Using three carefully screened quartz OSL ages, radiocarbon dating and site stratigraphic considerations we argue that the pIRIR$_{170}$ protocol can be used to produce reliable age estimates. Fading rates for the pIRIR$_{170}$ signal are consistently low (average g$_{2days}$: 0.81 ± 0.58). The pIRIR$_{170}$ residuals are dose dependent (r^2 = 0.58); but are consistently low as a proportion (e.g. 1–4%) of sample equivalent dose (D$_e$). Despite the water-lain depositional context, single aliquot D$_e$ distributions tend toward normality (for 11/19 samples) irrespective of aliquot size (2 mm or micro-aliquots containing 2–30 grains) with only a few statistical outliers per sample (max. n = 3) and overdispersion (OD) ranging from 1.6 to 30% excluding the two youngest (late Holocene) samples (OD: 37–87%). The resulting pIRIR$_{170}$ ages are in the correct stratigraphic order and illustrate the potential of pIRIR$_{170}$ luminescence dating to investigate the timing, processes and drivers of fluvial system adjustments across the Karoo.

1. Introduction

Alluvial and colluvial sediments in tectonically stable settings like the South African Karoo constitute important archives of fluvial/slope system adjustments (Botha and Fedoroff, 1995; Marker, 1995; Holmes et al., 2003; Grenfell et al., 2014; Oldknow and Hooke, 2017) and, in some cases, late Quaternary climate change (Clarke et al., 2003; Lyons et al., 2014). Early applications of luminescence methods in such contexts included infrared stimulated luminescence (IRSL) and thermoluminescence (TL) dating of colluvial deposits of the Masotcheni formation on the Great Escarpment (Botha et al., 1994; Botha and Fedoroff, 1995; Wintle et al., 1993). These showed much promise based on good agreement with independent radiocarbon age control (e.g. Wintle et al., 1995a, 1995b). More recently, optically stimulated luminescence (OSL) dating of quartz has proven to be a reliable dosimeter for alluvial and colluvial deposition in the eastern Karoo (Rodnight et al., 2006; Keen-Zebert et al., 2013; Lyons et al., 2013), but the upper age limit is constrained at some sites by high environmental dose rates

(Clarke et al., 2003; Temme et al., 2008).

In contrast, Oldknow and Hooke (2017) sought to apply OSL dating to a complex alluvial and colluvial stratigraphy in the Wilgerbosch catchment, Sneeuberg (Fig. 1), but met with limited success. This was due variously to low quartz yields, a dim OSL signal, feldspar contamination, and/or OSL saturation (i.e. at less than 40 ka) caused by relatively high environmental dose rates (>4 Gy ka^{-1}). Therefore, an alternative luminescence chronometer needs to be considered.

The suitability of K-feldspar post-IR IRSL (pIRIR) methods for the dating of water-lain deposits has yet to be investigated in this part of the Karoo. This approach isolates a slower (or non) fading signal obtained via a second higher temperature IRSL signal administered after a lower temperature IRSL measurement (typically at 50 °C and denoted as IRSL$_{50}$; Thomsen et al., 2008; Buylaert et al., 2009, 2012). Despite the increased stability of the pIRIR signal relative to previously used IRSL$_{50}$ protocols, a number of studies have shown it bleaches more slowly than the IRSL$_{50}$ and quartz OSL signals (e.g. Godfrey-Smith et al., 1988; Buylaert et al., 2012, 2013; Kars et al., 2014; Colarossi et al., 2018;

Riedesel et al., 2018). This is of particular concern for sediments deposited in water-lain contexts (e.g. glacio-fluvial, fluvial, lacustrine) where equal sunlight bleaching of all grains cannot be guaranteed (Sohbati et al., 2012; Trauerstein et al., 2014; Smedley et al., 2015; Braumann et al., 2019; Carr et al., 2019). Yet, some studies from such environments have shown that even for late Holocene deposits, the pIRIR signals (e.g. pIRIR$_{170}$ and pIRIR$_{225}$) are sufficiently bleached and single aliquot results show excellent agreement with independent dating control (e.g. Ainscoe et al., 2019; Buckland et al., 2019; Smedley et al., 2019).

The basic compromise when selecting pIRIR stimulation temperatures is that while lower temperature post-IR stimulation (e.g. at 150 or 170 °C as opposed to 225 or 290 °C) may result in enhanced bleachability, lower residuals and therefore reduced risk of age over-estimation (e.g. Madsen et al., 2011; Lowick et al., 2012; Reimann et al., 2011, 2012; Kars et al., 2014; Colarossi et al., 2015); the risk of higher anomalous fading rates increases (Jain et al., 2015), potentially necessitating fading corrections (Huntley and Lamothe, 2001; Huntley, 2006).

Age overestimation may also not always result from poor bleaching. For example the size of the test dose employed during pIRIR measurements has been shown to result in dose recovery overestimation (e.g. for test doses <15% of D_e, Yi et al., 2016; Colarossi et al., 2018). Working on alluvial samples from the Moopetsi River, South Africa, Colarossi et al. (2015) generated pIRIR$_{225}$ ages that overestimated (>100%)

independent age (quartz OSL) control for samples older than 20 ka due to use of an unsuitably small test dose. However, the residuals in their study were not excessively high (11 ± 1.3 Gy) considering the chosen stimulation temperature and depositional context. Nevertheless, dating of young deposits (i.e. < 20 ka) in this and similar alluvial contexts may benefit from the use of a lower temperature pIRIR signal to minimize the size of the residual pIRIR as much as possible.

The aim of this paper is therefore to establish whether it is possible to identify and utilize a sufficiently bleached, non- or low-fading pIRIR signal capable of decoding the age structure of a complex alluvial/colluvial cut and fill sequence in the Wilgerbosch catchment. If successful, this would represent a significant breakthrough in demonstrating the potential of pIRIR to investigate fluvial landscape evolution possibly up to glacial-interglacial timescales in the wider Karoo region.

2. Study area

The Great Karoo is a vast (30% land surface of South Africa) dissected landscape of plains and flat-topped mountains, characterized by east-west orientated mountain ranges such as the Sneeuberg (Fig. 1A). The Sneeuberg lies within the eastern region of the warm temperate zone at a major climatic junction between summer- and winter-dominated rains (Sugden, 1989; Chase and Meadows, 2007). Average annual rainfall is ~423 mm and is concentrated in the late summer/early autumn (Grenfell et al., 2014). Diurnal and seasonal
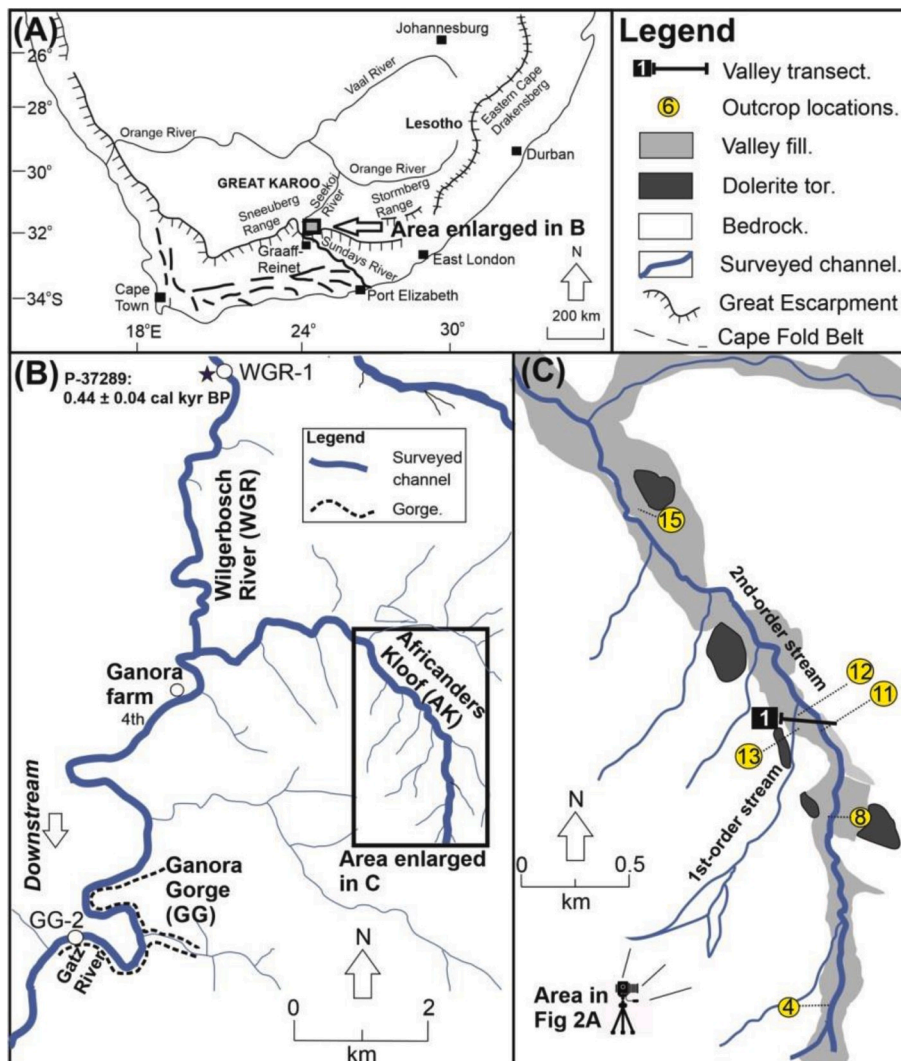

Fig. 1. (A) Map of Republic of South Africa highlighting the study area; (B) map of the Wilgerbosch catchment digitized from aerial photographs; (C) map of the low-order tributary "Africanders Kloof" showing locations of transects and outcrops selected for pIRIR dating, dolerite tors and surveyed limits of valley fills. Note: (i) the blue star at the top of the system denotes a radiocarbon age from outcrop WGR-1 (P-37289, see Fig. 3); (ii) outcrop GG-2 referred to throughout the text (see Fig. 9, Oldknow and Hooke, 2017).

temperatures show large fluctuations: summer maxima of ca. 30 °C in summer and winter minima of below −10 °C (Schultz, 1980). The Wilgerbosch catchment includes several low-order tributaries (Fig. 1B) which comprise the headwaters of the Sundays River (Fig. 1A). Africanders Kloof within Wilgerbosch is a mixed alluvial-bedrock stream incised into slopes of Balfour Formation (part of the Triassic-age Beaufort Group) sandstones and mudstones (Turner, 1978). These sedimentary rocks represent deposition in braided river and lacustrine settings. Plagioclase (e.g. anorthoclase) is more abundant than K-feldspars in these rocks (oligoclase, andesine and some microcline). Quartz occurs as mono- and polycrystalline varieties, the former tending to contain inclusions (Oghenekome, 2012). These sedimentary rocks are hypothesized to have been derived from eroding metamorphosized felsic volcanic rocks such as granitic gneisses (Bhatia, 1983).

These sedimentary strata are intruded by resistant Drakensberg Group dolerite sills and dikes. The dolerites are subalkaline tholeiitic basalts comprised of Ca-rich plagioclases (labradorite, bytownite, anorthite (in phenocrysts)), pyroxene, olivine, magnetite and skeletal ilmenite (Cox et al., 1967; Ramluckan, 1992; Neumann et al., 2011). Quartz is present only as an accessory mineral.

The vegetation of the study area is characterized by 'Eastern Upper Nama-Karoo (NKu2)' on gently sloping hills and is dominated by dwarf shrubs and grasses of the genera *Aristida* sp. and *Eragrostis* sp. Thin soils, stones and boulders on steeper sandstone slopes and dolerite ridges support dwarf Karoo shrubs and drought tolerant grasses (*Aristada sp., Eragrostis sp.,* and *Stipagrostis sp.*) of the 'Upper Karoo Hardeveld (NKu4)' (Mucina et al., 2006).

The basin is infilled by at least four extensive terrace fills in the higher order tributaries which have been interpreted as evidence of basin-wide cyclic cut and fill (Oldknow and Hooke, 2017). The low-order tributaries and upper slopes contain thick (6 m) colluvial deposits which are overlain by discontinuous flood-out deposits (outcrop AK-4, Figs. 1C and 3. Oldknow and Hooke (2017) obtained an OSL age (8.2 ± 1.5 ka) from a flood-out at outcrop AK-4 (see Figs. 1C and 3). The alluvial succession and locations of pIRIR samples are provided in Fig. 3. The sampling scheme ensured complete representation of the stratigraphy with a view to developing a chronology of cut and fill at the specified sites. The sedimentology and stratigraphy of deposits and locations of new luminescence dating samples are described as follows.

T1 comprises diamictic deposits up to 6 m thick in the Ganora Gorge. Vertically orientated, matrix-supported gravel-sized sandstone clasts attest to local slope rather than alluvial sedimentation. Oldknow and Hooke (2017) hypothesized these deposits accumulated due to colluvial activity during the Last Glacial Maximum.

T2 (outcrops AK12 and AK13) is characterized by two facies associations: 1) units composed of silty sand (unit A) and matrix-supported horizontally-bedded gravels (unit B) which display upward fining to sand (top of unit B); and 2) sandy silt units (units C–E) with evidence of disturbance by modern root channels within 1 m of the surface. These two facies groups are interpreted as channel deposits and overbank sediments respectively. An infilled palaeogully (unit F) is unconformably carved into unit E. A distinct rubified palaeosol horizon punctuates the succession (separating units B and C) and is indicative of a prolonged phase of geomorphic stasis. Vertical calcified root channels originating in unit C time-transgress this palaeosol unconformity intersecting with a calcrete horizon up to 10 cm thick, overprinting unit B. Micromorphological analyses have revealed that this calcrete is "rhizogenic" (Wright, 1990; Oldknow, 2016) and formed in association with a phreatic root system accessing an elevated water table (Wright et al., 1995).

T3 is only partially exposed at outcrop AK11 due to an inset deposit up to 2.4 m thick (T4). T3 consists of thick units of inversely graded silty sand (unit F1) and sandy silt (unit F2); buried by matrix-supported gravels (unit G). Oldknow and Hooke (2017) interpreted these facies as indicative of slopewash rather than channel or overbank sedimentation.

In contrast, T4 at profile AK11 is characterized by normally-graded,

horizontally-bedded units including matrix-supported gravels (units A and D), clast-supported cobbles (unit B), silty sands (unit C); and a relatively thick (~1 m) homogeneous sand unit (unit E) from which a quartz OSL age (AK11-1: 17 ± 2.5 ka) was obtained (Oldknow and Hooke, 2017). These deposits are interpreted as a migrating single-thread channel. In particular, the elevation and thickness of high-energy palaeo-flood deposits (unit B) corresponds to debris flow facies (e.g. AK8 unit D) in close proximity to an eroding dolerite tor (see Fig. 1C). On this basis, Oldknow and Hooke (2017) proposed that the aggradation recorded at T4 (AK11; this study) must have resulted from a phase of strong slope-channel connectivity (AK-8), implying that both the OSL and pIRIR ages for samples AK8-1 and AK11-1 ages should be concordant with one another.

T5 is characterized by well-sorted sandy silt (e.g. AK13 unit B2) or organic-rich silty sands containing plant macrofossils (e.g. AK15 unit B). It is interspersed with coarser gravel and sand units with inverse grading in the Wilgerbosch River. These facies indicate valley-floor wetland systems with low-energy channels that later incised due to land-use changes introduced during the European incursion (Boardman, 2014). An AMS ^{14}C age (P-37289; 0.44 ± 0.04 cal kyr BP, outcrop WGR-1, Fig. 2) was obtained from fossilized *Juncus* stems and provides a maximum age for the incision of these wetlands (Oldknow and Hooke, 2017). Rowntree (2013) and Boardman (2014) demonstrated gully erosion in this area was active at the start of the 20th century. Therefore, new pIRIR ages from AK13-1 and AK15-1 should bracket or overlap with this radiocarbon age.

Where possible samples for dating were obtained from relatively well-sorted homogeneous units of sandy silt or silty sand (13 of 19 samples). These are indicative of deposition in the lower-flow regime, either as slopewash (e.g. AK11-3), single-thread channels (e.g. AK11-1) or channel overbank (e.g. AK12-4) contexts.

Incomplete bleaching is most likely to be a challenge for samples collected from coarser (higher energy) channel deposits coupled with the shortest transportation distances (e.g. AK8-1). Samples collected from units previously subjected to waterlogging (e.g. AK12-6 to AK12-9; AK13-1) may also have been affected by variability in water content and external environmental dose. Indeed, a further advantage of using pIRIR methods in this context is the partial mitigation of these factors via the dose rate contribution from internal K and Rb.

3. Methods

The three ages previously reported (two quartz OSL, one ^{14}C) from the Wilgerbosch sequence offer a key benchmark against which to test pIRIR age reliability, especially the potential issue of bleaching. However, given the problems with quartz OSL in this area (Boardman et al., 2005; Oldknow, 2016), additional screening of the published OSL ages (samples AK4-1 and AK11-1, originally LV-509 and LV-515 in Oldknow and Hooke, 2017) as well as analysis of a new OSL sample (AK8-1) was undertaken to more thoroughly investigate the purity of the quartz. K-feldspar was then extracted from the same samples, dated with a low temperature pIRIR protocol and compared to the quartz OSL results.

3.1. OSL analyses

Preparation methods for OSL samples AK4-1 and AK11-1 were carried out at the University of Liverpool in 2015 and reported in detail in Oldknow (2016). In summary, 90–300 and 90–200 μm grains for AK4-1 and AK11-1 (respectively) were obtained via wet sieving. 10% v/v HCl and 30% v/v H_2O_2 were used to remove carbonates and organic matter. Density separation using sodium polytungstate provided the quartz fraction (2.62 < ρ < 2.76 g/cm^2). High feldspar contents (>50%) necessitated use of the large grain size windows and a strong (40% v/v for 40 min) HF etch to remove feldspar from the quartz fraction (Mauz and Lang, 2004). OSL analyses were conducted on a Risø DA-15 B/C reader equipped with 21 blue LEDs (470Δ30 nm; 80% of full diode
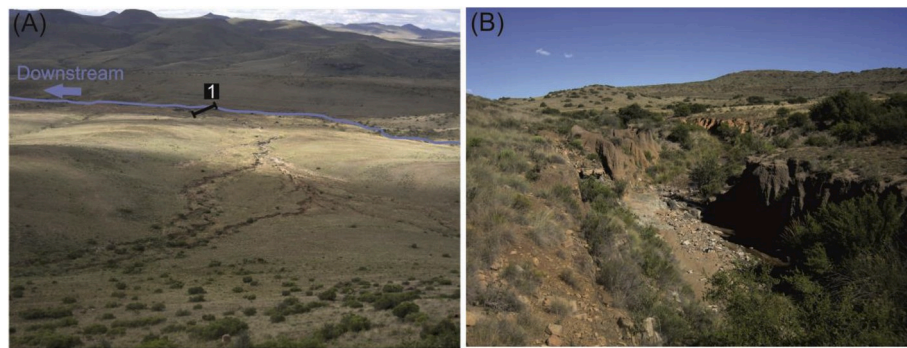
Fig. 2. Africanders Kloof: (A) Photograph of the catchment looking northeast taken from headwaters at location shown in Figure 1B, highlighted is transect 1; (B) Photograph of valley fills at transect 1, looking upstream.

current providing ~17 mW cm^{-2}). Measurements were carried out using the SAR protocol (Murray and Wintle, 2000) employing blue (125 °C) stimulation with luminescence detected through a Hoya U340 filter (transmitting 320–390 nm). The routine IR-depletion test to detect feldspar contamination was included (Duller, 2003). Data analysis was undertaken in Analyst v.4.31. Dose response curves (DRC) were fitted using a single saturating exponential function to obtain the best fit (reduced χ^2 parameter). D_e values were determined by integrating the initial 0.48s of the decay curves and subtracting the signal from a late background (10s).

Aliquots were rejected based on: (i) low OSL count rates (<300); (ii) recycling ratio >10% from unity; (iii) detection of feldspar contamination (IRSL depletion ratio <10%; Duller, 2003); (iv) failure to fit an exponential function to growth curve; and (v) recuperation >5%. SAR protocol suitability was tested using combined preheat/dose recovery tests. Oldknow (2016) found that dose recovery performance for AK4-1 was poor due to recuperation (Aitken and Smith, 1988) when using the standard SAR protocol. A dose recovery experiment was thus setup to test a variant of the SAR protocol which incorporated a high temperature OSL stimulation (in addition to the standard blue 125 °C stimulation) into the T_x part of the SAR cycle. For this dose recovery test, OSL stimulation temperature was varied from 200 to 280 °C (duration 40 s). An OSL stimulation temperature of 220 °C (for 40 s) coupled with a preheat of 200 °C and cutheat of 180 °C, was found to yield lowest recuperation values (e.g. <2%); and was employed to obtain 46 equivalent dose (D_e herein) estimates on 1 mm aliquots. For sample AK11-1, the standard SAR protocol (Murray and Wintle, 2000; Duller, 2003) was employed using a preheat of 240 °C and cutheat of 200 °C to obtain 61 D_e estimates on 1 mm aliquots (Oldknow, 2016).

Sample AK8-1 was prepared and measured at the University of Leicester using a Risø DA20 TL/OSL reader equipped with 28 blue LEDs (470Δ30 nm; 70% of full diode current providing ~70 mW cm^{-2}), with quartz luminescence detected through a Hoya U340 filter and IRSL through Schott BG39 and Corning 7–59 filters (also used to measure K-feldspar ages, section 3.2). This sample produced a relatively large quartz yield compared to AK4-1 and AK11-1, permitting use of a narrower grain size window (90–125 μm). A combined preheat/dose recovery test was used to verify the suitability of the SAR protocol (administered dose 43.6 Gy). A preheat of 220 °C and a cutheat of 200 °C (Fig. S1) resulted in best dose recovery (average 1.03 ± 0.02 n = 12). SAR protocol measurements (following Table S2a) produced 43 D_e estimates on 1 mm aliquots. Data analyses and integration limits used were the same as specified previously.

For all three OSL samples, few (<5%) aliquots exhibited IRSL indicative of 'feldspar' contamination; but certain kinds of K-rich feldspar (e.g. sanidine), Ca-rich (e.g. labradorite) and Na-rich (e.g. anorthoclase) plagioclases do not emit UV under IR excitation (Duller and Bøtter-Jensen, 1993; Mauz and Lang, 2004)

As such types of non-UV emitting feldspar are potentially present

given the geological context at Wilgerbosch (section 2.1), a series of alternative non-standard luminescence tests to screen for feldspar contamination were carried out: 1) Thermal quenching (cf. Wintle, 1975). A pure quartz sample exhibits "thermal quenching" with increased stimulation temperature (Duller et al., 1995) while feldspar exhibits "thermal assistance" (McKeever et al., 1997). A modified SAR protocol whereby the stimulation temperature was varied (from 50 to 325 °C at 20 °C intervals) was applied to 8 aliquots of each sample (Table S3). The resultant OSL versus stimulation temperature curves (Fig. S2) were fitted with the thermal quenching formula of McKeever et al. (1997) using the OriginPRO9 function fitter:

$$(1)\ I = I_0 \, / \, (1 \, + \, C \exp\left(-W/kT\right)$$

where W is the thermal activation energy, I is the OSL intensity, I_0 is the initial OSL intensity, k is the Boltzmann constant and C is a constant. Pure quartz should exhibit a W value of around 0.51 eV (with W values ~0.2 eV reported for feldspar (Wintle, 1975; Poolton et al., 2002; Shen et al., 2007).

2) The ratio of IR intensity to TL intensity at 110 °C (IR/TL herein) employed by Li et al. (2002). Most feldspars exhibit TL at 110 °C, but unlike quartz do not exhibit a single peak; rather they manifest as the rising limb (thermal assistance) of higher temperature TL peaks (McKeever et al., 1997). As only some feldspars emit UV under IR stimulation, but most feldspars exhibit thermal assistance (post 110 °C), the IR/TL ratio is more sensitive to polymineral mixtures than the IR-depletion test alone (Duller, 2003). Mauz and Lang (2004) demonstrated that IR/TL ratios approaching 0 are indicative of pure quartz, while IR/TL ratios closer to 1 indicate feldspar contamination. They cautioned however that as the IR/TL ratio only considers signal intensity at a specific temperature (110 °C), interpretation of the IR/TL ratio should be coupled with qualitative appraisal of the shape of the TL peak. Thus, we define two additional aliquot rejection criteria: 1) Aliquots which demonstrate thermal assistance (rather than thermal quenching) above 110 °C; and/or 2) IR/TL values > 0.25. In such instances, a QUANTAX micro-XRF (X-ray fluorescence) unit fitted to a Hitachi TM4000 benchtop scanning-electron microscope (SEM) was used to diagnose the nature of the contamination in both morphological and geochemical terms.

3.2. Post-IR IRSL methods

K-feldspar grains were extracted by treating each of the 19 samples with 10% v/v HCl and 32% v/v of H_2O_2 to remove carbonates and organics, respectively. Wet sieving isolated the coarsest fraction possible (controlled by sample amount) and was usually 180- or 212–250 μm (Table S1). Density separation utilizing sodium polytungstate provided the 2.53–2.58 g cm^{-3} K-rich feldspar fractions, which were then etched in 10% HF for 10 min 2 mm aliquots (several hundred grains) and micro-aliquots (2–30 grains) were analysed using a pIRIR protocol comprising
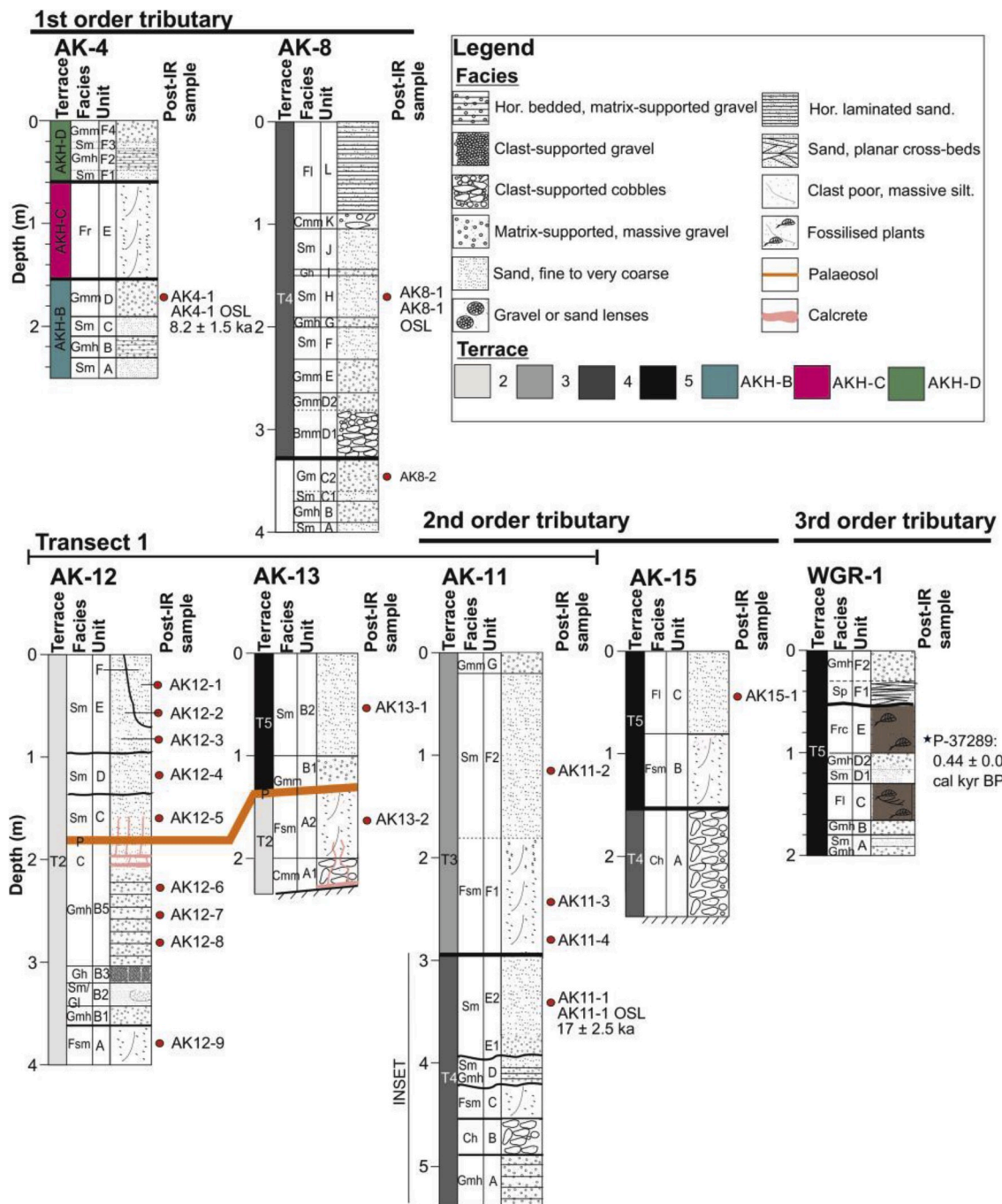
Fig. 3. Summary of the sedimentary succession at outcrops exposed in Wilgerbosch (see Fig. 1, for outcrop locations). Indicated are the locations of: (i) samples taken for pIRIR dating; (ii) existing quartz OSL ages (AK4-1, AK11-1); and (iii) a repurposed quartz OSL sample dated in this study (AK8-1). Note: radiocarbon age (0.44 ± 0.04 cal kyr BP) referred to throughout the text. Facies codes are modified from Miall (1996). Grain size terminology follows the Wentworth, 1922 scale. Some of the stratigraphic relations between these fills have been revised (from Oldknow and Hooke, 2017) in light of subsequent field observations. OSL prefix codes have been changed from LV- (as reported in Oldknow and Hooke, 2017) to AK- in this study for consistency.

a low temperature (50 °C) initial stimulation, followed by a high temperature (pIRIR) stimulation (Table S2b). IRSL for the 50 °C was measured for 100 s; IRSL for the high temperature stimulation was measured for 300 s. Samples were preheated for 60 s at a temperature set 30 °C above pIRIR stimulation temperature following Roberts (2012).

The choice of pIRIR stimulation temperature (150, 170, 225 and 290 °C) was then based on degree of overlap between the pIRIR ages (AK4-1, AK8-1, AK11-1, AK15-1) with independent age control (section 3.1; 4.1). The signal that exhibited the strongest overlap was then subjected to further analyses and ultimately applied to the remaining 15 samples.

A bleaching test was conducted (following Buckland et al., 2019) to assess the magnitude of the residual IR_{50} and pIRIR signals after different time intervals (i.e. 0, 10, 30, 60 min and 4 days) of exposure to direct (UK) sunlight (section 4.2).

Sensitivity of the chosen pIRIR signal to test dose size (13–60% of D_e) was assessed (section 4.3), while anomalous fading rates (section 4.4) were determined following Auclair et al. (2003) with g-values and corrections (following Huntley and Lamothe, 2001) determined using the R package "Luminescence" (Kreutzer et al., 2012).

Dose recovery tests (herein DRTs) and additional residual dose

measurements were performed to assess the robustness of the SAR protocol (section 4.5). Bleaching was achieved by exposing samples to natural UK daylight for 48 h. The administered beta dose was matched to the sample D_e and measured using the protocol outlined in Table S2b. Additionally, an "added dose" approach to dose recovery was used (Buylaert et al., 2011) which does not rely on complete bleaching of the sample prior to analysis.

Data analysis was undertaken in Analyst v.4.31. Dose response curves were fitted using a single saturating exponential function to obtain the best fit (reduced χ^2 parameter). D_e values were determined by integrating the initial 10s of the decay curves and subtracting the signal from a late background (30s). For all IRSL measurements, aliquots were only accepted if: (i) recycling ratio was ±10% of unity; (ii) recuperation was <5% of the natural dose; (iii) the error on the test dose signal was less than 3 standard deviations of the background signal; (iv) the uncertainty on the test dose luminescence measurement was less than 10%. Recuperation as a percentage of the natural signal was high for the very young sample AK15-1 (expected age between 0.1 and 0.5 kã) and aliquots exceeding 5% recuperation were still included in order to avoid potential overestimation of burial dose (D_b) (e.g. Buckland et al., 2019).

The resulting D_e distributions, utilizing all accepted aliquots are presented using Abanico plots (Dietze et al., 2016, Figs. S7, S8, S10). Identification and removal of D_e outliers (both OSL and pIRIR) was based on values lying outside 1.5 x the interquartile range (IQR) (Medialdea et al., 2014). After removal, D_e values were averaged using the central age model (CAM) (Galbraith et al., 1999). Two samples (AK12-9 and AK13-2) were used to investigate in more detail the sensitivity of D_e to aliquot size (section 4.6) via a comparison of ages obtained from micro-aliquot and 2 mm aliquot measurements.

3.3. Dose rate determination

Element concentrations were determined via inductively coupled plasma mass spectrometry (ICP-MS) for U and Th and ICP-OES for K, at the University of Leicester. U, Th and K concentrations were converted to annual dose rates following Guérin et al. (2011) with corrections for grain size (Mejdahl, 1979), water content (Aitken, 1985) and HF etching (Bell, 1979). For K-feldspar, the internal K and Rb dose rates assume grain K and Rb concentrations of 12.5 ± 0.5% and 400 ± 100 ppm respectively (Huntley and Baril, 1997; Huntley and Hancock, 2001). Cosmic dose rates were determined using the profile elevation (metres above sea-level, herein masl) and the measured sample depth (Prescott and Hutton, 1994) with a 5% relative uncertainty.

Final age uncertainties incorporate 3% relative uncertainties for each of the dose rate conversion factors, grain size attenuation and HF etching, propagated via standard methods. HF etching is assumed to have entirely removed the α-irradiated outer portion of the grains. The ICP-MS derived external beta dose rates were validated by comparison with beta dose rates obtained via GM beta counting. These show good correspondence (Fig. S3).

Taking the calcrete as a surrogate of the maximum upper limit of the palaeowater-table (section 2), an average burial water content of 15 ± 5% (Oldknow and Hooke, 2017) was used in age calculations for any samples below it (AK12-6 to AK12-9). For samples above the calcrete, the measured water content was used. A 5% change in water content results in a ~2000 year age difference for samples aged ~50 ka and ~1200 years for samples aged ~30 ka.

4. Results

4.1. Quartz OSL verification tests and OSL ages

Table 1 indicates that thermal activation values (W) for each of the quartz samples are consistent with published values for pure quartz (e.g. 0.51 eV, Shen et al., 2007). Two aliquots of AK4-1 were 'atypical' ($W = 0.36$ eV) but still higher than published values for feldspar (e.g. 0.19 eV,

Table 1

Range and mean values of selected OSL-based parameters (thermal activation energy W; IR/TL ratio) to assess quartz purity.

Sample	W range	W mean	IR/TL range	IR/TL mean
AK4-1	0.36–0.70	0.56	0.02–0.24	0.07
AK8-1	0.41–0.66	0.50	0.04–0.27	0.12
AK11-1	0.45–0.57	0.49	0.05–0.65	0.20

Shen et al., 2007).

The TL curves for each sample possess 110 °C peaks that are typical of quartz (Fig. S4a). Exceptions include three aliquots of AK4-1 (Fig. S4b - red line). Sample AK11-1 is notably more problematic, as a stable background post-110 °C is not reached for >75% of all aliquots. For 9 aliquots, the TL observed at 110 °C does not occur as a single peak, but as a thermally assisted rising limb of a higher temperature peak indicative of feldspar (Fig. S4b). Six of these nine aliquots also exhibit IR/TL values > 0.25 that are consistently higher than AK4-1 and AK8-1 (Table 1) and correspond to IR/TL values indicative of feldspar contamination (Li et al., 2002; Mauz and Lang, 2004). When D_e is plotted as a function of IR/TL for these aliquots (Fig. S5), a weak inverse (−0.28, p < 0.05) correlation is observed, which, in conjunction with the shape of the TL curve, indicates a 'faded' feldspar luminescence signal.

SEM analyses of etched quartz grains (AK11-1) adjudicates on the question of the contamination registered by the luminescence-based tests. Observations include Na and Mg-rich opaque and translucent grains in conjunction with "glassy" transparent Si-rich (quartz) grains (Fig. S6) indicating either inclusions within the quartz or feldspar grains. On this basis, the aforementioned nine aliquots of AK11-1 were rejected and the sample age recalculated in comparison to the published age.

To summarize, samples AK4-1 and AK8-1 exhibit quartz OSL characteristics that justify their use as a benchmark against which to test pIRIR protocol performance and pIRIR signal bleaching. AK11-1 is contaminated, but the clear TL 110 °C peak exhibited by 52/61 aliquots attests to the overall dominance (in luminescence terms) of suitable quartz.

The OD for the AK8-1 D_e is quite high (21%) considering both the grain size (90–125 μm) and aliquot size of this sample, but is moderately skewed (0.99) by three high outliers (>60 Gy). Removal of these outliers and recalculation of the central age model (CAM) D_e moves the age from 15.6 ± 0.8 ka to 15.0 ± 0.8 ka and lowers the OD to 17% (Table 2; Fig. S7). Seven statistical outliers were identified for AK11-1 (Fig. S7). Their removal moves the CAM age from 15.4 ± 2.6 ka to 14.7 ± 2.6 ka and lowers the OD to 16% (Table 2).

4.2. pIRIR signal selection

The suitability of different elevated temperature post-IR stimulations (i.e. pIRIR$_{150, 170, 225, 290}$) was assessed by comparing the results for K-rich feldspar fractions extracted from samples AK4-1, AK8-1 and AK11-1 with their corresponding quartz OSL age control (Table 2, Fig. 4).

Fig. 4 shows that the pIRIR$_{150}$ ages underestimate the OSL ages, while the pIRIR$_{225}$ and pIRIR$_{290}$ tend to overestimate the OSL ages.

Table 2

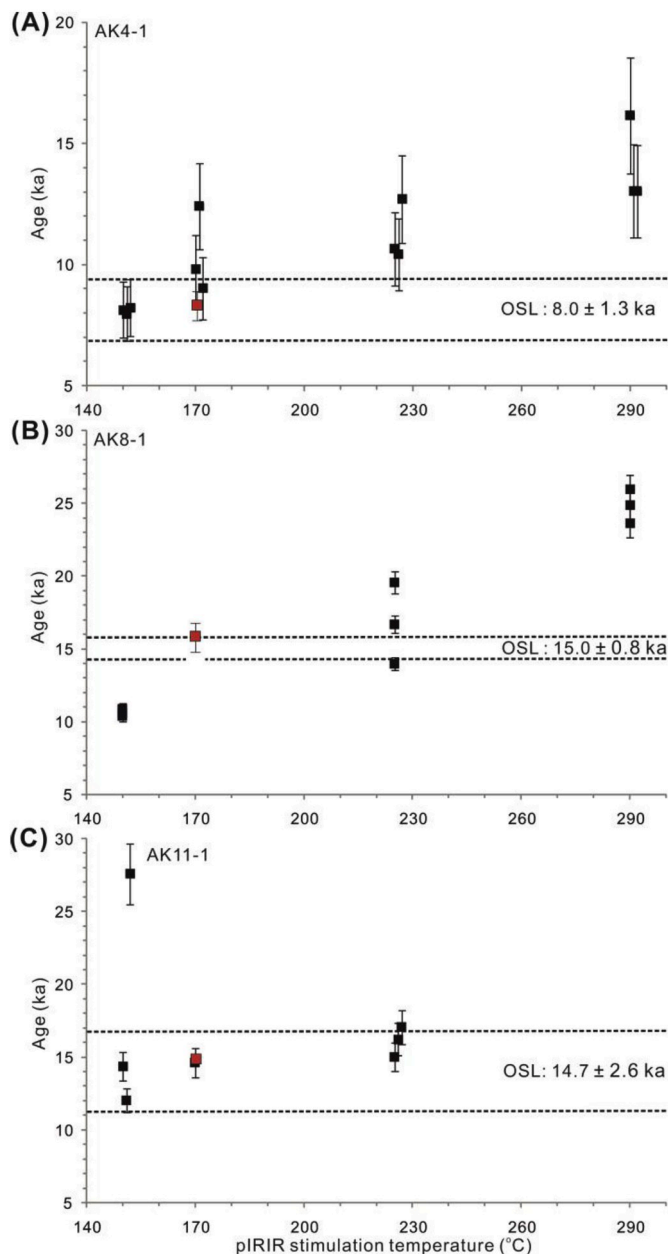Results of quartz OSL analyses and revised ages.

Sample	n[a]	σ_{OD} (%)[b]	D_e (Gy)[c]	Final age (ka) (1 σ)
AK4-1	43	32	33.8 ± 1.7	8.0 ± 1.3
AK8-1	43	21	38.4 ± 2.0	15.6 ± 0.8
	[d]40	[d]17	[d]37.0 ± 1.1	[d]15.0 ± 0.8
AK11-1	52	24	55.8 ± 1.9	15.4 ± 2.6
	[d]45	[d]16	[d]53.4 ± 1.3	[d]14.7 ± 2.6

[a] Number of aliquots used in final age calculation.

[b] Overdispersion parameter.

[c] Central Age Model D_e.

[d] Recalculated D_e and OD values after outlier removal (Fig. S7).

Fig. 4. Fading-uncorrected pIRIR ages (ka) obtained from 2 mm aliquot measurements for different pIRIR stimulation temperatures. Note: (i) red squares denotes CAM pIRIR$_{170}$ ages (based on 12, 13 and 14 aliquots respectively) which overlap the quartz ages (1σ error); (ii) 3 aliquots at the other stimulation temperatures were measured; (iii) the pIRIR$_{290}$ was not measured for AK11-1 based on its tendency to overestimation.

pIRIR$_{290}$ age AK8-1 significantly overestimates (~50%) the OSL age. In contrast, the pIRIR$_{170}$ and OSL ages for all three samples show consistent overlap.

Fig. 5 shows the pIRIR$_{170}$ luminescence behaviour and D$_e$ distributions. Results are expanded to include pIRIR$_{170}$ data from a fourth sample (AK15-1) which comes from a stratigraphic horizon coeval with radiocarbon age P-37289 (section 2). Despite the larger D$_e$ of samples AK8-1 and AK11-1 (up to 63.6 ± 1.2 Gy) compared to AK15-1 and AK4-1 (up to 41.1 ± 1.2 Gy), the IRSL signals are not especially bright (max. ~7000 counts). This could be a consequence of less "potassic" K-feldspar variants (e.g. sanidine) within the sediments at Wilgerbosch (section 3).

The D$_e$ distributions presented in Fig. 5 range from normal (AK4-1, AK11-1) to positively skewed due to 1–2 high outlier aliquots (see also

Table S6: AK8-1, AK15-1). AK15-1 is overdispersed (87%), but exhibits a small D$_e$ (2.2 ± 0.6 Gy). Despite a single high outlier for AK15-1 (29.2 Gy), its CAM pIRIR$_{170}$ age (0.6 ± 0.3 ka) is in good agreement with ^{14}C age P-37289 (0.44 ± 0.04 cal kyr BP).

Sample AK4-1 exhibits an OD of 17%. Removal of a single low outlier (19 Gy) reduces OD (7.3%) and moves the CAM pIRIR$_{170}$ age from 8.2 ± 0.5 ka to 8.6 ± 0.3 ka (Table 4). AK8-1 is rather more dispersed (OD: 30%) considering its (2 mm) aliquot size, but removal of two high outliers (89 and 151 Gy) brings its pIRIR$_{170}$ age from 18 ± 1.5 ka to 16.1 ± 0.4 ka, which is in better agreement (1 σ error) with the OSL age (Fig. 4, Tables 2 and 4). Sample AK11-1 exhibits very low OD (6.4%).

Fig. 6 demonstrates that more than 1 h of sunlight exposure is required to reduce the natural pIRIR$_{170}$ signal of sample AK12-8 to less than 33% of its original intensity (from a dose of 222 Gy). In contrast the natural IR$_{50}$ signal intensity is reduced by ~90% (of 133 Gy) after 30 min (1.8 × 10^3 s). After 4 days of light exposure, the pIRIR$_{170}$ signal was reduced to 4% (8.9 Gy) and the IR$_{50}$ to 1% (1.3 Gy) of their original signals. This equates to residual ages of 2.1 ka and 0.3 ka respectively (dose rate 4.21 Gy/ka, Table S1). This pIRIR$_{170}$ residual age is four times greater than that of AK15-1 (Table 4) and 25% the magnitude of age AK8-1; yet both of these ages are concordant with independent age control. This is considered further in section 4.5.

In summary, as the pIRIR$_{170}$ signal produces ages in strong agreement with independent age control and bleaches quickly, a pIRIR protocol comprising a 50 °C IRSL stimulation followed by a subsequent 170 °C stimulation was used (Table S2b) in subsequent experiments, and to determine K-feldspar luminescence ages.

4.3. Test dose size

Fig. 7 shows little variation in sample age is observed with changing test dose size (13–60% of D$_e$), although precision tends to be higher (see AK4-1 and AK11-2) for moderate test doses (22–32%). Thus, a ~30% test dose was applied to all SAR measurements (Table S2b).

4.4. Anomalous fading

Table 3 and S4 show fading rates (g$_{2days}$) for 17 of the 19 pIRIR$_{170}$ and IR$_{50}$ samples respectively. The pIRIR$_{170}$ fading rates are 0.29 ± 1.06%, 0.75 ± 0.54% and 0.15 ± 0.36% for samples AK4-1, AK8-1 and AK11-1 respectively. Consistently low g-values were obtained for all samples (average g$_{2days}$ value 0.81 ± 0.58%, max 1.76% per decade, WGK4-1) removing the need for fading correction (Huntley and Lamothe, 2001). The IR$_{50}$ fading rates are non-trivial (average 2.58 ± 0.6%). Fading is 2.48 ± 0.52%, 2.15 ± 0.59% and 4.95 ± 0.51% per decade for samples AK4-1, AK8-1 and AK11-1 respectively. Fading correction brings the IR$_{50}$ ages into strong (e.g. AK4-1) and better (e.g. AK8-1, AK11-1) agreement with both the pIRIR$_{170}$ and OSL ages (Fig. 8, Table 2 and S5).

The effectiveness of the fading correction method (e.g. Huntley and Lamothe, 2001), however, is contingent upon sample D$_e$ residing on the linear part of the DRC. As illustrated in Fig. 5, the D$_e$ of the older samples (e.g. AK11-1) lies on the exponential part of the DRC which may account for the tendency of the fading-corrected IR$_{50}$ ages to underestimate the pIRIR$_{170}$ ages above ~15–20 ka (Fig. 8A). For the oldest sample (e.g. AK8-2), the underestimation of the fading-uncorrected IR$_{50}$ is >50% (Fig. 8B).

4.5. Suitability of the pIRIR$_{170}$ SAR protocol

Table 3 and S4 summarize results of residual dose and dose recovery experiments for the pIRIR$_{170}$ and IR$_{50}$ signals respectively. Table 4 and S5 summarize pIRIR$_{170}$ and IR$_{50}$ D$_e$ and ages respectively. Aliquot acceptance using standard SAR criteria was consistently high (>80%) irrespective of aliquot size (2 mm aliquots or micro-aliquot).

The pIRIR$_{170}$ residual doses are dose-dependent (Li et al., 2013) and
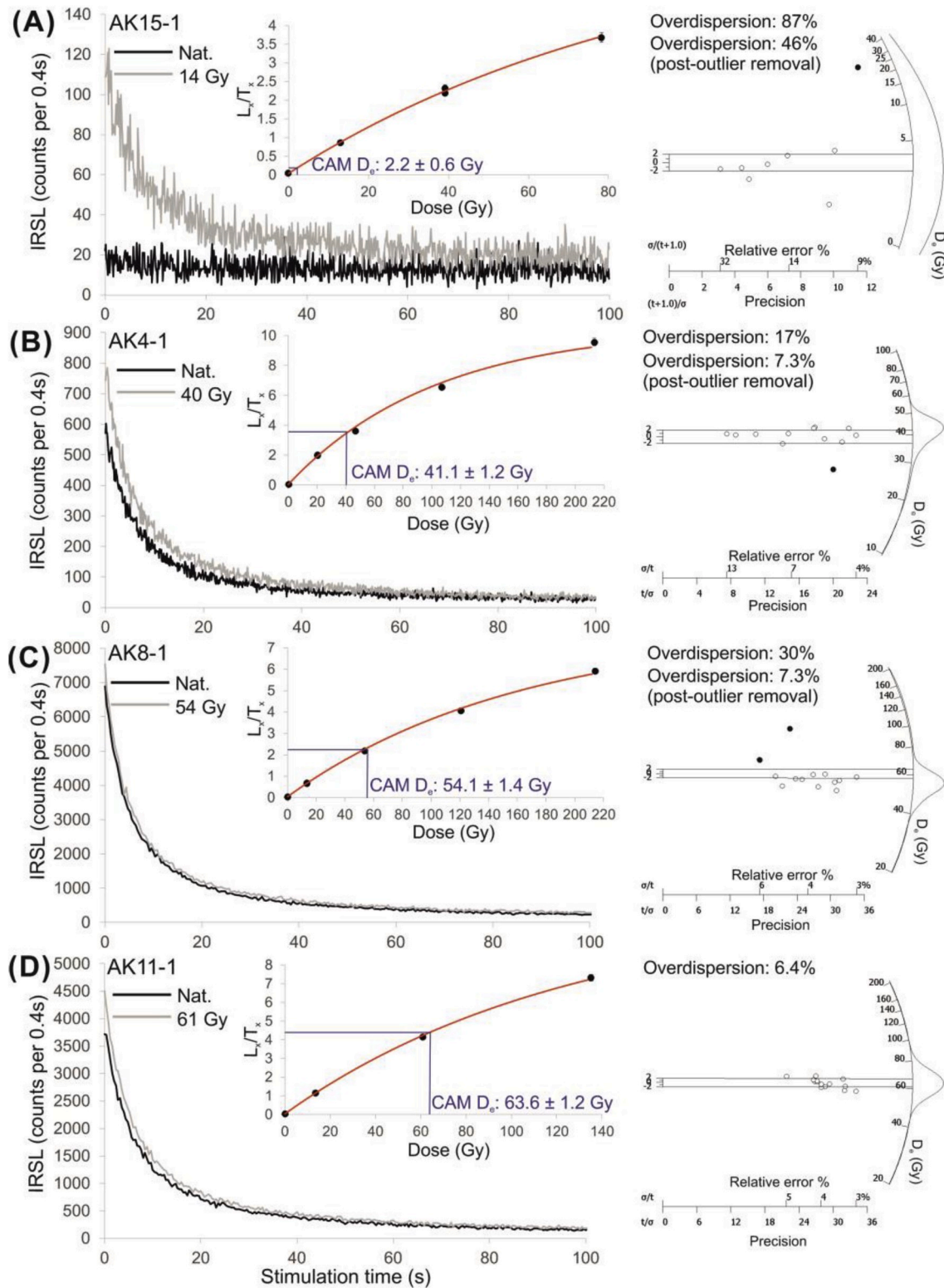
Fig. 5. Shine-down curves, dose response curves (fitted using a single saturated exponential function) and radial plots for the pIRIR$_{170}$ measurements on (A) AK4-1, (B) AK8-1, (C) AK11-1 and (D) AK15-1. Samples are ranked from youngest (AK15-1) to oldest (AK11-1). Outlier D$_e$ values are marked in black. Note: AK15-1 D$_e$ data are based on micro-aliquot measurements; the other samples were measured using 2 mm aliquots.

range from 1 to 4% of sample D$_e$ except AK12-8, the residual dose of which is ~9% (Fig. S10). The DRR of sample AK12-8 after bleaching in natural light overestimated (DRR of 1.14 ± 0.02) the given dose (220 Gy); but the added dose experiment yielded a DRR close to unity (1.03 ± 0.01). Sample AK12-7 from the same stratigraphic unit exhibited a much

smaller residual dose (6.31 ± 1.09 Gy; ~3% of D$_e$) and good dose recovery (added dose DRR: 0.95 ± 0.05), yet its D$_e$ overlaps with AK12-8 (Table 4). Since the D$_e$ of sample AK12-8 does not appear to incorporate a large residual (~9% of D$_e$ or 20 Gy) relative to sample AK12-7 (from the same stratigraphic unit), we propose that the dose recovery

Table 3

Internal checks of pIRIR$_{170}$ protocol performance carried out on 2 mm aliquots. Note: (i) dose recovery ratios (DRR) are average values using all measured (n = 3) aliquots; (ii) AK8-2 and AK12-X were subjected to two DRTs using low and high administered doses; (iii) AK12-X was used during preliminary testing and not dated.

Sample	DRR Natural Light	DRR Added dose	g$_{2days}$ (% per decade)	Residual dose (Gy).
AK4-1	–	–	0.29 ± 1.06	–
AK8-1	0.99 ± 0.04	–	0.75 ± 0.54	2.30 ± 0.16
AK8-2	–	1.01 ± 0.02 (66.9 Gy) 0.89 ± 0.04 (401.5 Gy)	0.10 ± 0.47	6.23 ± 1.19
AK11-1	–	–	0.15 ± 0.36	–
AK11-2	0.96 ± 0.01 [a]1.12 ± 0.03	–	0.99 ± 0.50	3.00 ± 0.50
AK11-3	1.09 ± 0.04	–	0.68 ± 0.56	3.88 ± 0.83 [a]6.95 ± 0.91
AK11-4	–	–	–	–
AK12-1	0.97 ± 0.02	–	1.61 ± 0.38	–
AK12-2	1.04 ± 0.04	0.97 ± 0.03	0.89 ± 0.71	–
AK12-3	–	0.95 ± 0.03	0.85 ± 0.49	5.72 ± 0.15 [a]9.40 ± 1.40
AK12-4	–	0.88 ± 0.02	0.79 ± 0.65	–
AK12-5	0.93 ± 0.00	–	0.62 ± 0.44	4.00 ± 0.70
AK12-6	–	–	0.73 ± 0.62	–
AK12-7	–	0.95 ± 0.05	1.22 ± 0.74	6.31 ± 1.09 [a]11.33 ± 1.13
AK12-8	1.14 ± 0.02	1.03 ± 0.01	0.98 ± 0.61	20.60 ± 2.20
AK12-9	–	–	0.01 ± 0.57	–
WGK4-1	0.96 ± 0.01	–	1.76 ± 0.71 [a]0.83 ± 0.43	4.20 ± 0.30 [a]8.80 ± 3.30
AK12-X	–	1.04 ± 0.01 (65.4 Gy) 0.94 ± 0.01 (366.3 Gy)	0.53 ± 0.49	–
Average	**1.01 ± 0.01**	**0.95 ± 0.05**	**0.81 ± 0.58**	**6.30 ± 0.64** [a]**9.12 ± 0.71**

[a] Refers to pIRIR$_{225}$ measurements given for comparative purposes.

overestimation for the former reflects inadequate bleaching conditions under natural daylight (Buckland et al., 2019). Excluding AK12-8, the sample with the largest residual is thus AK8-1, which is 4% of its D$_e$ or 0.7 ka. Subtraction of this residual makes no difference to the pIRIR$_{170}$ age. which overlaps with the faster-bleaching quartz OSL age (Fig. 4). The residuals were therefore not subtracted from sample D$_e$ values in this study (following Li et al., 2013).

Of the 12/19 samples measured for dose recovery, 9 exhibited good pIRIR$_{170}$ dose recovery performance. Sample AK8-2 has the highest D$_e$ (501 Gy) and although it is not saturated, a high administered beta dose (402 Gy) resulted in dose recovery underestimation (0.89 ± 0.04). A smaller administered dose (67 Gy) yielded a DRR at unity (1.01 ± 0.02). A similar underestimation was observed for a comparatively young (e.g. AK12-4) sample (0.88 ± 0.02) whose age was consistent with other samples (e.g. AK12-3 and AK13-2) from the same stratigraphic unit that showed good dose recovery (Table 3).

4.6. pIRIR$_{170}$ D$_e$ distributions

Fig. 9 compares micro-aliquot and 2 mm aliquot pIRIR$_{170}$ D$_e$ values for two samples. The degree of inter-aliquot scatter in pIRIR$_{170}$ D$_e$ values increases down to the micro-aliquot (i.e. <5 grain) level, but the average D$_e$ essentially remains the same. As a result, the CAM D$_e$ (even if 3–4 grains are measured, see AK13-2) is comparable with the 2 mm aliquot CAM D$_e$ data. In addition, Table 4 shows that the ages determined using different aliquot sizes for these two samples overlap within 1σ. The same is true of the bracketing ages, irrespective of aliquot size.

The results of 2 mm aliquot and micro-aliquot D$_e$ determinations are presented in Table 4 and Fig. S9. Skewness and kurtosis in relation to OD are presented in Table S6. In general, and as expected, 2 mm aliquot D$_e$s

Table 4

Results of pIRIR$_{170}$ D$_e$ measurements for 2 mm aliquots (top) and micro-aliquots (bottom). Shown on the left are the number of aliquots measured over the number passing the rejection criteria (n/n), the observed OD, the CAM D$_e$ and resulting CAM ages. Shown on the right are the number of statistical outliers removed (N) and the resulting final OD, CAM D$_e$ and CAM ages (ka). Note: Samples dated using both 2 mm and micro-aliquots (AK12-9 and AK13-2) are emboldened for comparison. They overlap within 1σ implying insensitivity of D$_e$ to aliquot size.

| Sample	All accepted aliquots				Post-outlier removal			
	n/n	OD %	CAM D$_e$ (Gy)	Age (ka)	N	OD %	CAM D$_e$ (Gy)	Age (ka)
2 mm aliquots								
AK4-1	12/13	17	39.2 ± 2.1	8.2 ± 0.5	1	7.3	41.1 ± 1.2	8.6 ± 0.3
AK8-1	13/14	30	60.7 ± 5.1	18.0 ± 1.5	2	7.8	54.1 ± 1.4	16.1 ± 0.4
AK8-2	7/7	11	501.1 ± 24.0	121.3 ± 5.8	1	9.3	485.0 ± 22.0	117.4 ± 5.3
AK11-1	14/15	6.4	63.6 ± 1.2	14.3 ± 0.3	–	–	–	–
AK11-2	18/18	4.9	122.5 ± 1.8	25.3 ± 1.4	2	1.2	122.4 ± 1.2	25.3 ± 1.4
AK11-3	13/13	7.5	127.0 ± 3.0	29.6 ± 2.4	–	–	–	–
AK12-1	12/12	4.0	14.5 ± 0.4	4.4 ± 0.4	–	–	–	–
AK12-5	18/18	4.8	184.8 ± 3.2	37.2 ± 2.2	–	–	–	–
AK12-8	13/16	1.6	221.8 ± 11.0	52.7 ± 1.8	–	–	–	–
AK12–9	**7/7**	**9.6**	**208.0 ± 10.5**	**51.4 ± 2.6**	**1**	**1**	**217.4 ± 2.4**	**53.7 ± 2.6**
AK13–2	**12/12**	**6.2**	**178.8 ± 3.8**	**41.9 ± 3.8**	**1**	**3.5**	**175.9 ± 2.8**	**41.2 ± 2.8**
Micro-aliquots								
AK11-4	18/22	29	126.9 ± 8.7	30.8 ± 2.1	2	9.7	138.3 ± 3.8	33.6 ± 0.9
AK12-2	24/24	28	165.3 ± 9.6	39.0 ± 2.3	3	14	164.4 ± 5.6	38.9 ± 1.2
AK12-3	18/18	21	186.9 ± 9.8	42.3 ± 2.2	2	9.3	189.2 ± 5.3	42.8 ± 1.2
AK12-4	14/18	22	167.0 ± 10	37.5 ± 2.2	2	15	156.7 ± 7.4	35.2 ± 2.9
AK12-6	13/13	21	238.0 ± 15	53.7 ± 3.4	2	17	224.0 ± 12	50.6 ± 2.7
AK12-7	10/13	14	224.0 ± 12	49.0 ± 2.6	2	6.9	224.1 ± 8.1	49.0 ± 1.9
AK12–9	**17/18**	**18**	**202.8 ± 9.4**	**50.1 ± 2.3**	**-**	**-**	**-**	**-**
AK13-1	13/17	37	6.9 ± 0.7	1.6 ± 0.2	2	14	6.0 ± 0.3	1.4 ± 0.2
AK13–2	**13/16**	**29**	**162.0 ± 14**	**37.9 ± 3.3**	**2**	**11**	**167.5 ± 7.4**	**39.2 ± 1.7**
AK15-1	8/14	87	3.2 ± 1.3	0.6 ± 0.3	1	46	2.2 ± 0.6	0.4 ± 0.1

are less dispersed (OD: 1.6–30%, average 6.4%) compared to the micro-aliquot D$_e$s (OD: 14–87%, average 26%). The pIRIR$_{170}$ OD values are comparable with those from the IR$_{50}$ D$_e$ distributions, but are higher for four samples (AK11-4, AK12-2, AK12-4 and AK13-2, see Table 4 and S5). CAM D$_e$s range from 3 to 501 Gy, tend to be fairly normally distributed (skewness <1 for 11/19 samples) and possess only a few outliers (max. 3 per sample). The impact of these outliers on the pIRIR$_{170}$ CAM ages is small. They usually consist of 1–2 high outlier aliquots (e.g. AK12-2; AK15-1), but are sometimes counterbalanced by a low outlier of similar magnitude (e.g. AK12-2) or in a few cases a very low (i.e. > 3 x IQR) outlier (e.g. AK11-4). AK11-4 is negatively skewed (−1.67) and dispersed (29%) due to two such low outliers, which after removal lowers the OD (9.7%) and moves the CAM age from 30.8 ± 2.1 to 33.6 ± 0.9 ka. Notably, the resultant CAM ages for all samples are in correct stratigraphic order and consistent with stratigraphy (Figs. 3 and 10).
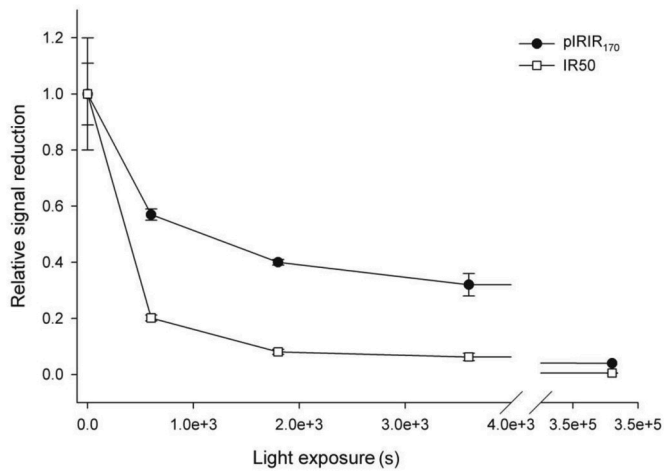
Fig. 6. Results of bleaching experiment in direct UK sunlight using a sample (AK12-8) with a large D_e (pIRIR$_{170}$: 222 Gy; IR$_{50}$: 133 Gy). Residual IR$_{50}$ and pIRIR$_{170}$ signal measured after 0, 10, 30, 60 min and 4 days (3.5e+5 s).
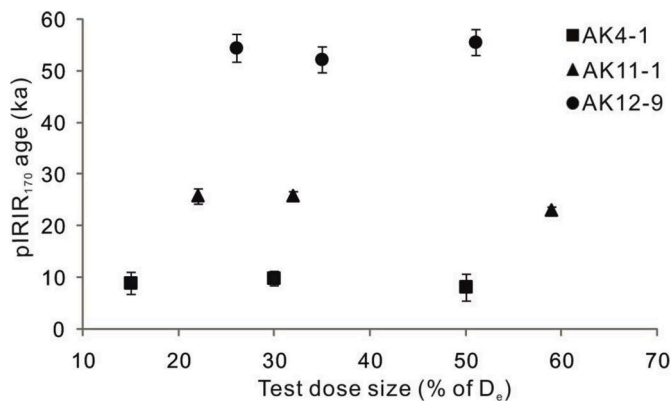
Fig. 7. Impact of test dose size (% of D_e) on pIRIR$_{170}$ ages.
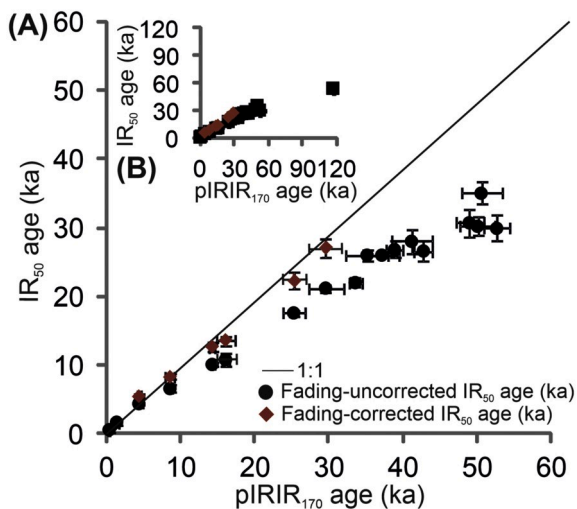
Fig. 8. (A) Comparison of IR$_{50}$ ages before and after fading correction (Huntley and Lamothe, 2001) with pIRIR$_{170}$ ages. Highlighted are samples constrained by independent age control (Fig. 5); (B) Inset includes the oldest sample (AK8-2, see Table 4). Note tendency for fading-corrected IR$_{50}$ ages to slightly underestimate the pIRIR$_{170}$ ages >15 ka.
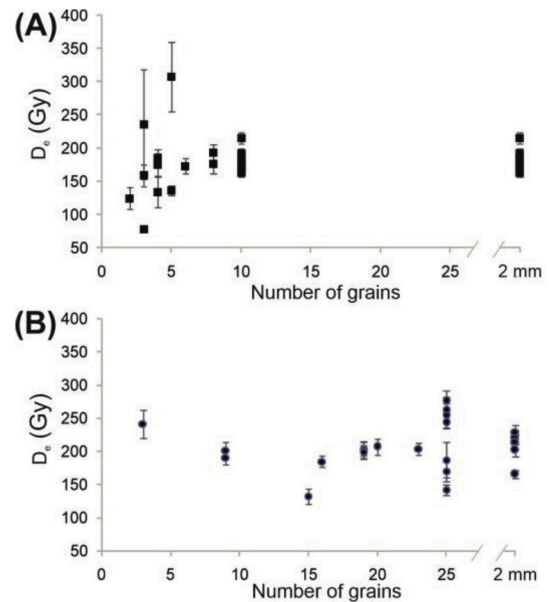
Fig. 9. Equivalent doses (D_e) plotted as a function the number of grains per aliquot for samples AK13-2 (A) and AK12-9 (B). Note: Two sets of ages for AK13-2 and AK12-9 are reported in Table 4 based on micro-aliquot (2–25 grains) and 2 mm aliquots.

5. Discussion

5.1. Overall performance of the pIRIR$_{170}$ protocol

The strong overlap between the pIRIR$_{170}$, quartz OSL (Fig. 4), fading-corrected IR$_{50}$ ages (Fig. 8) and ^{14}C age P-37285 (section 4.2) indicates that the necessary pre-condition for bleaching (for the pIRIR$_{170}$) of around or less than ~2 days sunlight exposure (section 4.5) has been most completely achieved for facies deposited under subcritical flow conditions.

For facies deposited under high-energy flow conditions coupled with having been eroded from a nearby source (sample AK8-1), there is a slight overestimation of the pIRIR$_{170}$ age compared to the OSL age, but this is substantially less pronounced than for ages obtained using higher temperature post-IR stimulations (pIRIR$_{225}$, pIRIR$_{290}$). The pIRIR$_{290}$, which bleaches the most slowly (Smedley et al., 2019), appears unsuitable in this catchment (Fig. 4). While the pIRIR$_{225}$ demonstrated reasonable overlap with independent age control (e.g. AK4-1, AK11-1), Table 3 shows that the residuals are still higher on average (7% of D_e) than the pIRIR$_{170}$, similar to published values (11 ± 1.3 Gy, cf. Colarossi et al., 2015). Coupled with the fact the pIRIR$_{170}$ is non-faded, the pIRIR$_{170}$ is preferable in this catchment. The pIRIR$_{225}$ could potentially be utilized for dating older deposits (e.g. sample AK8-2: >100 ka) where the pIRIR$_{170}$ may underestimate D_b.

Furthermore, if during successive phases of valley filling sediments with a low rather than high D_b were reworked, this would have also helped mitigate against the potential limitations for sunlight bleaching imposed by short transport distances and flow hydraulics. As bleaching appears to be non-limiting for the youngest samples (<15 ka), it follows that the relative impact of any partially-bleached grains was proportionally smaller for the majority of the pIRIR$_{170}$ ages which are older than 25 ka.

We now consider the performance of the pIRIR$_{170}$ protocol on the basis of internal checks (Table 3). In general, the high aliquot acceptance rate and good dose recovery indicates the pIRIR$_{170}$ SAR protocol is suitable for determining the D_b of these alluvial samples. The reason for DRR underestimation for AK8-2 is however unclear. This could be due to inadequate characterization of the DRC of this sample, considering its
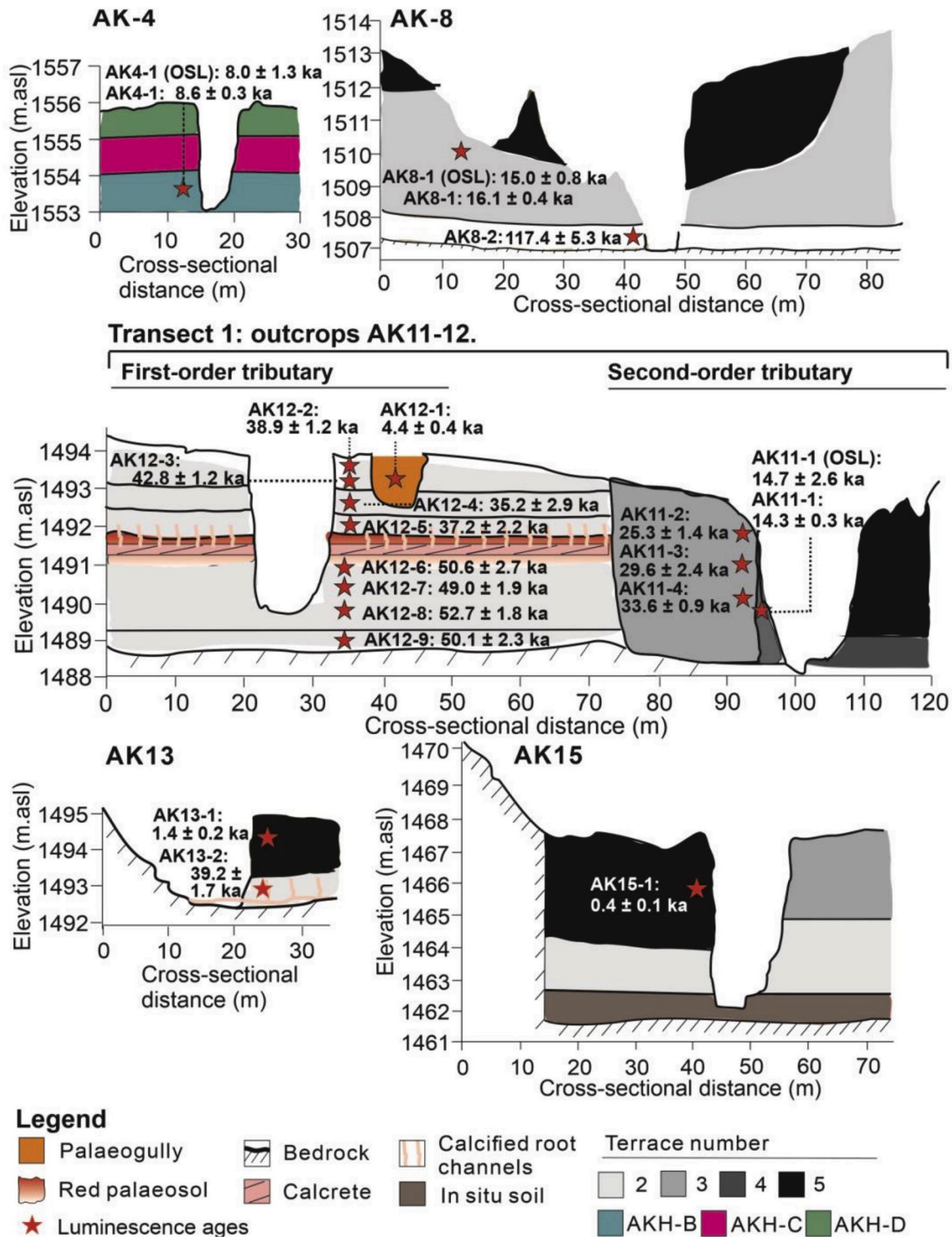
Fig. 10. Chronostratigraphy of the alluvial/colluvial succession comprising 3 quartz OSL and 19 new pIRIR$_{170}$ ages (see Tables 2 and 4). Note: 1) ages reported omit statistical outliers as outlined in the text; 2) all luminescence ages are pIRIR$_{170}$ except those labeled 'OSL'; and 3) see Fig. 1C for locations of outcrops/transects.

very high D$_e$. However, the fact that a comparable given dose of 366 Gy can be successfully recovered for another sample (e.g. AK12-X) implies that the pIRIR$_{170}$ protocol may be suitable for dating sediments in these valleys up to at least ~85–90 ka old.

The DRR overestimation in concert with the high residual dose measured for sample AK12-8 is most likely explicable in terms of varied bleaching conditions under natural daylight (e.g. Buckland et al., 2019). Were its large residual (20.6 ± 2.2 Gy–9% of D$_e$) representative of an

unusually large unbleachable signal for this sample, we would expect to see an excursion in the sample age relative to the bracketing ages, which is not the case.

5.2. Impact of aliquot size on pIRIR$_{170}$ D$_e$

The fact that the IR$_{50}$ and pIRIR$_{170}$ D$_e$ values exhibit relatively few statistical outliers is a further indication that partial bleaching is non-

limiting in this instance (Trauerstein et al., 2014). The observation that micro-aliquots (Fig. 9) exhibit clear signals (>3 sigma above background) implies that signal averaging may equally not be serious, but a full single grain analysis would be required to assess the degree of grain-to-grain signal variation (Rhodes, 2015). What is clear is that the distribution of micro-aliquot D_e values does not appear to differ greatly to that of the 2 mm aliquot D_e analyses. This - coupled with the further observations that there is strong agreement between: (i) pIRIR$_{170}$ ages based on 2 mm aliquot measurements and independent age control (section 4.1); and (ii) ages irrespective of aliquot size within the same stratigraphic unit (e.g. section AK12) - suggests that 2 mm aliquot CAM D_e values provide a reliable estimate of D_b. That the sample D_es appear to be reproducible using relatively few grains may attest to the higher efficiency of K-feldspar relative to quartz grains in representing the total population of D_e values within a given sample (Smedley et al., 2019).

5.3. Sources of scatter in pIRIR$_{170}$ D_e distributions

OD is aliquot-size dependent, increasing at the micro-aliquot scale (Fig. S9). Sample AK8-1 is the only example of a 2 mm aliquot pIRIR$_{170}$ age exhibiting high OD (~30%) most likely due to inclusion of partially bleached grains (section 5.1). Indeed, although several high D_e outliers were observed for other samples (e.g. AK12-2 to AK12-6, AK15-1), the associated OD (except the youngest samples) was always lower than AK8-1 even when micro-aliquots were used (e.g. AK13-2: OD 29%). Ages from profile AK12 overlap, irrespective of the presence of such outliers.

The second possible extrinsic contributor to OD is bioturbation (Jankoswki et al., 2015). Post-deposiGuérin et al., 2011tional mixing may be responsible for the low D_e outliers observed for samples AK4-1, AK11-4, AK12-2 to AK12-4 (Table 4; Fig. S9), as these sediments are friable, with physical evidence of disturbance by modern root channels in places. Intrusion of sand grains is not deemed likely immediately above and below the calcrete, based on micromorphological evidence which shows illuviation of just clay and silt grains (Oldknow, 2016).

The observation that D_e scatter increases down to the micro-aliquot scale (i.e. <10 grains, e.g. AK13-1) may indicate that sample OD is incorporating the effects of intrinsic factors (i.e. variations in K content, fading and microdosimetry), but an analysis of single grains would be required to assess their relative contributions (Rhodes, 2015).

In summary, sample OD tends to largely reflect few individual outliers, the presence of which makes minimal difference to the resulting CAM pIRIR$_{170}$ ages. Application of the outlier removal procedure (section 3.2) reduced OD to well below 20% except for the youngest sample (Table 4).

5.4. pIRIR$_{170}$ chronology of "cut and fill" and its implications

The final pIRIR$_{170}$ ages are presented in Fig. 10 and all are consistent with their stratigraphic positions. The samples collected from AK12 (T2) indicate two alluvial aggradational episodes at 51 ± 2 ka and 39 ± 2 ka (averages) punctuated by a phase of geomorphic stasis reflected in the palaeosol horizon. Taking the difference between these averages, this stasis must have been sustained over a period of at least 8 ka. Rhizogenic calcrete formation commenced ~39 ± 2 ka. These ages also indicate that the deposits comprising T1 (section 2.1) which were originally hypothesized to be LGM (Oldknow and Hooke, 2017), must in fact be older than 50 ka, possibly deposited during Marine Isotope Stage (MIS) 4.

The samples from T3 indicate a comparatively 'slow' phase of colluviation, with 2 m of deposition from 33.6 ± 0.9 to 25.3 ± 1.4 ka (ages AK11-4 to AK11-2). Given the age of the lowest sample (AK11-4), it is possible that the onset of aggradation coincided with floodplain sedimentation on T2 (AK12). This would imply that T2 in the first-order tributary did not incise, possibly as a result of the armouring effect of the calcrete .

The two samples collected from T4 are indicative of alluvial channel

aggradation at 16.1 ± 0.4 ka (AK8-1) and 14.3 ± 0.3 ka (AK11-1) in late MIS 2. Although there are currently no bracketing samples from either profile, these ages are in close agreement (2σ) and consistent with morpho-stratigraphic correlations (Oldknow and Hooke, 2017).

A notable feature of the new chronostratigraphy is the lack of an early-mid Holocene record. The small palaeogully incised into T2 is the only deposit to yield a mid-Holocene age (AK12-1: 4.4 ± 0.4 ka). The samples collected from the fine-grained vlei (wetland) deposits (T5) date to 1.4 ± 0.2 ka (AK13-1) and 0.4 ± 0.1 ka (AK15-1), consistent with the morphostratigraphic model of Oldknow and Hooke (2017) (their T4). These are at least 50% younger than the youngest vleis (2.5 ± 0.05 ka cal BP) reported in the nearby Klein Seekoi River (Holmes et al., 2003).

The chronology therefore indicates three phases of aggradation (~51, ~39, and ~33–25 ka) and an incision phase (~37–34 ka) in MIS 3 where channel cutting exceeded terrace thickness. A key control on whether aggradation occurs is the degree of connectivity between thick weathering mantles on dolerite tors and/or colluvial deposits at various locations (e.g. GG-2, Fig. 1B) with the channel network. There may be connectivity when either (i) the valley floors are not buffered from the slopes by terrace deposits or (ii) there is gully headcutting into the slopes triggering a "sediment slug" (Oldknow and Hooke, 2017).

The potential role for climate in driving such episodes of connectivity has, until now, been untestable at Wilgerbosch. It is intriguing that the timing of palaeosol and wetland (48–41 ka) and wetland (~39 ka) development corresponds to dry (~46–41 ka) and relatively wet periods (41–28 ka) in the South African interior (Lyons et al., 2014). Colluviation in this period has been reported by Temme et al. (2008) in the Okhombe valley, and by Rowell et al. (2018) in the Stormberg Range (~35.2 ± 2.6 ka - 29.8 ± 3.1 ka), overlapping with the Wilgerbosch record (~33–25 ka, T3). The absence of MIS 2 and MIS 1 deposits at Wilgerbosch is the subject of ongoing investigation. Elsewhere in South Africa, the LGM was characterized by reduced (Keen-Zebert et al., 2013) or no sediment accumulation (Temme et al., 2008; Rowell et al., 2018), perhaps due to aridity (Lyons et al., 2014). However, Oldknow and Hooke (2017) suggested that the cementation of the oldest deposits (i.e. T1-T2) coupled with limited storage space at Africanders Kloof, could have led to disproportionate representation of the early part of the terrace record at the expense of younger fills. This may account for the limited expression of late MIS 2 (e.g. AK8-1, AK11-1) and Holocene (e.g. AK13-1, AK15-1) deposits in contrast to other nearby sites (e.g. Bousman et al., 1988; Sugden, 1989; Marker, 1995; Holmes et al., 2003).

6. Conclusions

Nineteen samples from alluvial and colluvial cut and fill sediments were dated via the application of 2 mm aliquot and micro-aliquot pIRIR$_{170}$ measurements. Non-standard luminescence based tests to screen for non-UV emitting feldspar contaminants were carried out on three OSL samples, yielding three acceptable OSL ages which served (in conjunction with one ^{14}C date) as vital independent age control to validate the pIRIR$_{170}$ ages. The pIRIR$_{170}$ protocol yields ages in substantially better agreement with fading-corrected IR$_{50}$, quartz-OSL and ^{14}C ages than the pIRIR$_{225}$ and especially the pIRIR$_{290}$ protocols, suggesting the latter signals are insufficiently bleached in this context. The resulting pIRIR$_{170}$ ages are in the correct stratigraphic order, are non-faded and exhibit lower residual doses than the pIRIR$_{225}$. Single aliquot D_e distributions for the pIRIR$_{170}$ tend toward normality irrespective of aliquot size, with few outliers and OD typically ranging from 1.6 to 30% excluding the very youngest samples (OD 37–87%). The adequacy of bleaching is potentially facies dependent, and it is interesting that the only sample showing clear evidence of partial bleaching (AK8-1) originated from a high-energy deposit in an alluvial fan context. The stability of the CAM D_es across aliquot sizes implies signal averaging masking heterogeneous bleaching is not a serious issue for these samples. Overall it seems that the pIRIR$_{170}$ signal is suitable for dating deposits up to at least MIS 4. With this detailed chronology we can begin to

consider the Africanders Kloof terrace record in the context of climate driven patterns of aggradation, geomorphic stasis and wetland formation during MIS 3.

Declaration of competing interest

None.

Acknowledgements

Appendix A. Supplementary data

Supplementary data to this article can be found online at https://doi.org/10.1016/j.quageo.2020.101064.

References

Ainscoe, E.A., Abdrakhmatov, K.G., Baikulov, S., Carr, A.S., Elliott, A.J., Grützner, Walker, R.T., 2019. Variability in surface rupture between successive earthquakes on the Suusamyr Fault, Kyrgyz Tien Shan: implications for palaeoseismology. Geophys. J. Int. 216, 703–725.
Aitken, M.J., 1985. Thermoluminescence Dating. Academic Press, London, p. 359.
Aitken, M.J., Smith, B.W., 1988. Optical dating: Recuperation after bleaching. Quaternary Science Reviews 7 (3), 387–393.
Auclair, M., Lamothe, M., Huot, S., 2003. Measurement of anomalous fading for feldspar IRSL using SAR. Radiat. Meas. 37, 487–497.
Bell, W.T., 1979. Attenuation factors for the absorbed radiation dose in quartz inclusions for thermoluminescence dating. Ancient TL 8, 1–12.
Bhatia, M.R., 1983. Plate tectonics and geochemical composition of sandstone. J. Geol. 9, 611–627.
Boardman, J., 2014. How old are the gullies (dongas) of the Sneeuberg uplands, Eastern Karoo, South Africa? Catena 113, 79–85.
Boardman, J., Holmes, P.J., Rhodes, E.J., Bateman, M.D., 2005. Colluvial fan gravels, depositional environments and luminescence dating: a Karoo case study. S. Afr. Geogr. J. 87 (1), 73–79.
Botha, G.A., Fedoroff, N., 1995. Palaeosols in late quaternary colluvium, northern KwaZulu-natal, South Africa. J. Afr. Earth Sci. 21 (2), 291–311.
Botha, G.A., Wintle, A.G., Vogel, J.C., 1994. Episodic late Quaternary palaeogully erosion in northern KwaZulu-Natal, South Africa. Catena 23 (3–4), 327–340.
Bousman, C.B., Partridge, P.C., Scott, L., Metcalfe, S.E., Vogel, J.C., Seaman, M., Brink, J.S., 1988. Palaeoenvironmental implications of late pleistocene and Holocene valley fills in Blydefontein basin, noupoort, C.P. South Africa. Palaeoecol. Afr. 19, 43–67.
Braumann, S.M., Neuhuber, S., Fiebig, M., Schaefer, J.M., Hintersberger, E., Lüthgens, C., 2019. Challenges in constraining ages of fluvial terraces in the Vienna basin (Austria) using combined isochron burial and pIRIR225 luminescence dating. Quat. Int. 509, 87–102.
Buckland, C.E., Bailey, R.M., Thomas, D.S.G., 2019. Using post-IR IRSL and OSL to date young (< 200 yrs) dryland aeolian dune deposits. Radiat. Meas. 126, 1–12.
Buylaert, J.-P., Murray, A.S., Thomsen, K.J., Jain, M., 2009. Testing the potential of an elevated temperature IRSL signal from K-feldspar. Radiat. Meas. 44, 560–565.
Buylaert, J.-P., Jain, M., Murray, A.S., Thomsen, K.J., Thiel, C., Sohbati, R., 2012. A robust feldspar luminescence dating methods for Middle and Late Pleistocene sediments. Boreas 41, 435–451.
Buylaert, J.-P., Thiel, C., Murray, A.S., Vanderberghe, D., Yi, S., Lu, H., 2011. IRSL and post-IR IRSL residual doses recorded in modern dust samples from the Chinese Loess Plateau. Geochronometria 38, 432–440.
Buylaert, J.-P., Murray, A.S., Gebhardt, A.C., Sohbati, R., Ohlendorf, C., Thiel, C., Wastegard, S., Zolitschka, B., The PASADO Science Team, 2013. Luminescence dating of the PASADO core 5022-1D from Laguna Potrok Aike (Argentina) using IRSL signals from feldspar. Quat. Sci. Rev. 71, 70–80.
Carr, A.S., Hay, A.S., Powell, D.M., Livingstone, I., 2019. Testing post-IR IRSL luminescence dating methods in SW Mojave Desert, California, USA. Quat. Geochronol. 49, 85–91.
Chase, B.M., Meadows, M.E., 2007. 'Late Quaternary dynamics of southern Africa's winter rainfall zone. Earth Sci. Rev. 84 (3–4), 103–138.
Clarke, M.L., Vogel, J.C., Botha, G.A., Wintle, A.G., 2003. Late Quaternary hillslope evolution recorded in eastern South African colluvial badlands. Palaeogeogr. Palaeoclimatol. Palaeoecol. 197 (3–4), 199–212.
Colarossi, D., Duller, G.A.T., Roberts, H.M., 2018. Exploring the behaviour of luminescence signals from feldspars: implications for the Single Aliquot Regenerative dose protocol. Radiat. Meas. 109, 35–44.
Colarossi, D., Duller, G.A.T., Roberts, H.M., Tooth, S., Lyons, R., 2015. Comparison of paired quartz and feldspar post-IR IRSL dose distributions in poorly bleached fluvial sediments from South Africa. Quat. Geochronol. 30, 233–238.
Cox, K.G., Macdonald, R., Hornung, G., 1967. Geochemical and petrologic provinces in the Karoo basalts of southern Africa. Am. Mineral. 52, 1451–1474.
Dietze, M., Kreutzer, S., Burow, C., Fuchs, M.C., Fischer, M., Schmidt, C., 2016. The abanico plot: visualising chronometric data with individual standard errors. Quat. Geochronol. 31, 12–18.
Duller, G.A.T., 2003. Distinguishing quartz and feldspar in single grain luminescence measurements. Radiat. Meas. 37 (2), 161–165.
Duller, G.A.T., Bøtter-Jensen, L., 1993. 'Luminescence from potassium feldspars stimulated by infrared and green light. Radiat. Protect. Dosim. 47 (1–4), 683–688.
Duller, G.A.T., Bøtter-Jensen, L, Poolton, N.R.J., 1995. Stimulation of mineral-specific luminescence from multi-mineral samples. Radiation Measurements 24, 87–93.
Galbraith, R.F., Roberts, R.G., Laslett, G.M., Yoshida, H., Olley, J.M., 1999. Optical dating of single and multiple grains of quartz from jinmium rock shelter, northern Australia: Part I, experimental design and statistical models. Archaeometry 41, 339–364.
Godfrey-Smith, D.I., Huntley, D.J., Chen, W.-H., 1988. Optical dating studies of quartz and feldspar sediment extracts. Quat. Sci. Rev. 1, 373–380.
Grenfell, S.E., Grenfell, M.C., Rowntree, K.M., Ellery, W.N., 2014. Fluvial connectivity and climate: a comparison of channel pattern and process in two climatically contrasting fluvial sedimentary systems in South Africa. Geomorphology 205, 142–154.
Guérin, G, Mercier, N, Adamiec, G, 2011. Dose-rate conversion factors: update. Ancient TL 29, 5–8.
Holmes, P.J., Boardman, J., Parsons, A.J., Marker, M.E., 2003. Geomorphological palaeoenvironments of the Sneeuberg range, Great Karoo, South Africa. J. Quat. Sci. 18 (8), 801–813.
Huntley, D.J., 2006. 'An explanation of the power-law decay of luminescence. J. Phys. Condens. Matter 18 (4), 1359–1365.
Huntley, D.J., Baril, M.R., 1997. The K content of the K-feldspars being measured in optical dating or in thermoluminescence dating. Ancient TL 15, 11–13.
Huntley, D.J., Hancock, R.G.V., 2001. The Rb contents of the K-feldspar grains being measured in optical dating. Ancient TL 19, 43–46.
Huntley, D.J., Lamothe, M., 2001. Ubiquity of anomalous fading in K-feldspar and the measurement and corrections for it in optical dating. Can. J. Earth Sci. 38, 1093–1106.
Jain, M., Buylaert, J.P., Thomsen, K.J., Murray, A.S., 2015. Further investigations on "non-fading" in K-Feldspar. Quat. Int. 362, 3–7.
Jankoswki, N.R., Jacobs, Z, Goldberg, P, 2015. 'Optical dating and soil micromorphology at MacCauley's beach, New South Wales, Australia. Earth Surf. Process. Landforms 40, 229–242.
Kars, R.H., Reimann, T., Wallinga, J., 2014. Are feldspar SAR protocols appropriate for post-IR IRSL dating? Quat. Geochronol. 22, 126–136.
Keen-Zebert, A., Tooth, S., Rodnight, H., Duller, G.A.T., Roberts, H.M., Grenfell, M., 2013. Late Quaternary floodplain reworking and the preservation of alluvial sedimentary archives in unconfined and confined river valleys in the eastern interior of South Africa. Geomorphology 185, 54–66, 0.
Kreutzer, S., Schmidt, C., Fuchs, M.C., Dietze, M., Fisher, M., Fuchs, M., 2012. Introducing an R package for luminescence dating analysis. Ancient TL 30, 1–7.
Li, B, Jacobs, Z, Roberts, R.G., Li, S.H., 2013. Extending the age limit of luminescence dating using the dose-dependent sensitivity of MET-pIRIR signals from K-feldspar. Quaternary Geochronology 17, 55–67.
Li, S.H., Sun, J.M., Zhao, H., 2002. Optical dating of dune sands in the northeastern deserts of China. Palaeogeogr. Palaeoclimatol. Palaeoecol. 181, 419–429.
Lowick, S.E., Trauerstein, M., Preusser, F., 2012. Testing the application of post-IR IRSL dating to fine grain waterlain sediments. Quat. Geochronol. 8, 33–40.
Lyons, R., Tooth, S., Duller, G.A., 2013. Chronology and controls of donga (gully) formation in the upper Blood River catchment, KwaZulu-Natal, South Africa: evidence for a climatic driver of erosion. Holocene 23 (12), 1875–1887.
Lyons, R., Tooth, S., Duller, G.A., 2014. Late Quaternary climatic changes revealed by luminescence dating, mineral magnetism and diffuse reflectance spectroscopy of river terrace palaeosols: a new form of geoproxy data for the southern African interior. Quat. Sci. Rev. 95, 43–59.
Madsen, A.T., Buylaert, J.P., Murray, A.S., 2011. Luminescence Dating of Young Coastal Deposits from New Zealand Using Feldspar. Geochronometria 38, 379–390.
Marker, M.E., 1995. Late Quaternary environmental implications from sedimentary sequences at 2 high-altitude Lesotho sites. South Afr. J. Sci. 91 (6), 294–298.
Mauz, B, Lang, A, 2004. Removal of the feldspar-derived luminescence component from polymineral fine silt samples for optical dating applications: evaluation of chemical treatment protocols and quality control procedures. Ancient TL. 22 (1), 1–8.
McKeever, S.W.S, Bøtter-Jensen, L, Agersnap Larsen, N, Duller, G.A.T, 1997. Temperature dependence of OSL decay curves: Experimental and theoretical aspects. Radiation Measurements 27 (2), 161–170.
Medialdea, A., Thomsen, K.J., Murray, A.S., Benito, G., 2014. Reliability of equivalent-dose determination and age-models in the OSL dating of historical and modern palaeoflood sediments. Quat. Geochronol. 22, 11–24.
Mejdahl, V., 1979. Thermoluminescence dating: beta attenuation in quartz grains. Archaeometry 21, 61–73.
Miall, A.D., 1996. The Geology of Fluvial Deposits: Sedimentary Facies, Basin Analysis and Petroleum Geology.. Springer-Verlag, Berlin, p. 79.

Mucina, L, Rutherford, M.C., Palmer, A.R., Milton, S.J., Scott, L, Wendy-Lloyd, J, van der Merwe, B, Hoare, D.B., Bezuidenhout, H, Vlok, J.H.J., Euston-Brown, D.I.W., Powrie, L.W., Dold, A.P., 2006. Nama-Karoo biome. The Vegetation of South Africa, Lesotho and Swaziland. South African National Botanical Institute, Pretoria, pp. 324–347.

Murray, A.S., Wintle, A.G., 2000. Luminescence dating of quartz using an improved single-aliquot regenerative-dose protocol. Radiat. Meas. 32 (1), 57–73.

Neumann, E.R., Svensen, H., Galerne, C.Y., Planck, S., 2011. Multistage evolution of dolerites in the Karoo large igneous province, central South Africa. J. Petrol. 52 (5), 959–984.

Oghenekome, M.E., 2012. Sedimentary Environments and Provenance of the Balfour Formation (Beaufort Group) in the Area between Bedford and Adelaide, Eastern Cape Province, South Africa. MSc thesis. University of Forte Hare, Alice, South Africa.

Oldknow, C.J., 2016. Late Quaternary Landscape Evolution in the Great Karoo, South Africa: Processes and Drivers. PhD thesis. University of Liverpool, Liverpool, UK.

Oldknow, C.J., Hooke, J.M., 2017. Alluvial terrace development and changing landscape connectivity in the Great Karoo, South Africa. Insights from the Wilgerbosch River catchment, Sneeuberg. Geomorphology 288, 12–38.

Poolton, N.R.J., Wallinga, J, Murray, A.S., Bulur, E., Bøtter-Jensen, L, 2002. Electrons in feldspar I: on the wavefunction of electrons trapped at sample lattice defects. Physics Chemistry Minerals 29, 210–216.

Prescott, J.R., Hutton, J.T., 1994. Cosmic ray contributions to dose rates for luminescence and ESR dating: large depths and long term variations. Radiat. Meas. 23, 497–500.

Ramluckan, V.R., 1992. The Petrology and Geochemistry of the Karoo Sequence Basaltic Rocks in the Natal Drakensberg at Sani Pass. MSc thesis. University of Durban-Westville, South Africa.

Reimann, T., Tsukamoto, S., 2012. 'Dating the recent past (< 500 years) by post-IR IRSL feldspar - examples from the north sea and Baltic sea coast. Quat. Geochronol. 10 (10), 180–187.

Reimann, T., Tsukamoto, S., Naumann, M., Frechen, M., 2011. 'The potential using K-rich feldspars for optical dating of young coastal sediments – a test case from Darss-Zingst peninsula (southern Baltic Sea coast). Quat. Geochronol. 6 (2), 207–222.

Rhodes, E., 2015. Dating sediments using potassium feldspar single-grain IRSL: initial methodological considerations. Quat. Int. 362, 14–22.

Riedesel, S., Brill, D., Roberts, H.M., Duller, G.A.T., Garrett, E, Zander, A.M., King, G.F., Tamura, T., Burow, C, Cunningham, A, et al., 2018. Single-grain feldspar luminescence chronology of historical extreme wave event deposits recorded in a coastal lowland, Pacific coast of central Japan. Quaternary Geochronology 45, 37–49.

Roberts, H.M., 2012. Testing Post-IR IRSL protocols for minimising fading in feldspars, using Alaskan loess with independent chronological control. Radiat. Meas. 47, 716–724.

Rodnight, H., Duller, G.A.T., Wintle, A.G., Tooth, S., 2006. Assessing the reproducibility and accuracy of optical dating of fluvial deposits. Quat. Geochronol. 1 (2), 109–120.

Rowell, A.L.K., Thomas, D.S.G., Bailey, K.M., Holmes, P.J., 2018. Sand ramps as palaeoenvironmental archives: integrating general principles and regional contexts through reanalysis of the Klipkraal sands, South Africa. Geomorphology 311, 103–113.

Rowntree, K., 2013. The evil of sluits: a re-assessment of soil erosion in the Karoo of South Africa as portrayed in century-old sources. Journal of Environmental Management 130, 98–105.

Schultz, B.R., 1980. Climate of South Africa, Part 9, General Survey. Weather Bureau, Department of Transport, Pretoria.

Shen, Z., Mauz, B., Lang, A., Bloemendal, J., Dearing, J., 2007. Optical dating of Holocene lake sediments: elimination of the feldspar component in fine silt quartz samples. Quat. Geochronol. 2 (1–4), 150–154.

Smedley, R.K., Buylaert, J.-P., Újvári, G., 2019. Comparing the accuracy and precision of luminescence ages for partially-bleached sediments using single grains of K-feldspar and quartz. Quat. Geochronol. 53, 101007.

Smedley, R.K., Duller, G.A.T., Roberts, H.M., 2015. Assessing the bleaching potential of the 53 post-IR IRSL signal for individual K-feldspar grains: implications for single-grain dating. Radiation Measurements 79, 33–42.

Sohbati, R., Murray, A.S., Buylaert, J.-P., Ortuño, M., Cunha, P.P., Masana, E., 2012. April): 'Luminescence dating of Pleistocene alluvial sediments affected by the Alhama de Murcia fault (eastern Betics, Spain) – a comparison between OSL, IRSL and post-IR IRSL ages. Boreas 41, 250–262.

Sugden, J.M., 1989. Palaeoecology of the Central and Marginal Uplands of the Karoo. University of Cape Town, Cape Town, South Africa, p. 384.

Temme, A., Baartman, J.E.M., Botha, G.A., Veldkamp, A., Jongmans, A.G., Wallinga, J., 2008. Climatic controls on late Pleistocene landscape evolution of the Okhombe valley, KwaZulu-Natal, South Africa. Geomorphology 99 (1–4), 280–295.

Thomsen, K.J., Murray, A.S., Jain, M., Bøtter-Jensen, L., 2008. Laboratory fading rates of various luminescence signals from feldspar-rich sediment extracts. Radiat. Meas. 43, 1474–1486.

Trauerstein, M., Lowick, S.E., Preusser, F., Schlunegger, F., 2014. Small aliquot and single grain IRSL and post-IR IRSL dating of fluvial and alluvial sediments from the Pativilca Valley, Peru. Quat. Geochronol. 22, 163–174.

Turner, B.R., 1978. Sedimentary patterns of uranium mineralisation in the Beaufort group of the southern Karoo (gondwana) basin, South Africa. In: Miall, A.D. (Ed.), Fluvial Sedimentology, Canadian Association of Petroleum Geologists, Memoir, vol. 5, pp. 831–848.

Wintle, A.G., Li, S.H., Botha, G.A., 1993. Luminescence dating of colluvial deposits from Natal, South Africa. South Afr. J. Sci. 89, 77–82.

Wentworth, C.K., 1922. A scale of grade and class terms for clastic sediments. Journal of Geology 30, 377–392.

Wintle, A.G., 1975. Thermal quenching of thermoluminescence in quartz. Geophysics Journal of the Royal Astronomical Society. 41, 107–113.

Wintle, A.G., Botha, G.A., Li, S.H., Vogel, J.C., 1995a. A chronological framework for colluviation during the last 110kyr in KwaZulu/Natal. South Afr. J. Sci. 91, 134–139.

Wintle, A.G., Li, S.H., Botha, G.A., Vogel, J.C., 1995b. Evaluation of luminescence dating procedures applied to late-Holocene colluvium near St Paul's Mission, Natal, South Africa. Holocene 5, 97–102.

Wright, V.P., 1990. Estimating rates of calcrete formation and sediment accretion in ancient alluvial deposits. Geol. Mag. 127 (3), 273–276.

Wright, V.P., Platt, N.H., Marriott, S.B., Beck, V.H., 1995. A classification of rhizogenic (root-formed) calcretes, with examples from the Upper Jurassic-Lower Cretaecous of Spain and Upper Cretaceous of southern France. Sediment. Geol. 100 (1–4), 143–158.

Yi, S., Buylaert, J.-P., Murray, A.S., Lu, H., Thiel, C., Zeng, L., 2016. A detailed post-IR IRSL dating study of the Niuyangzigou loess site in north-east China. Boreas 45, 644–657.